HHS Public Access

Author manuscript

Prostate. Author manuscript; available in PMC 2016 October 01.

Published in final edited form as:

Prostate. 2015 October ; 75(14): 1620–1631. doi:10.1002/pros.23043.

Characterization of Autoimmune Inflammation Induced Prostate Stem Cell Expansion

Hsing-Hui Wang[a,b], **Liang Wang**[c], **Travis J. Jerde**[c], **Bin-Da Chan**[d,e], **Cagri A. Savran**[d,e], **Grant N. Burcham**[a,f], **Scott Crist**[a,b], and **Timothy L. Ratliff**[a,b,1]

[a]Department of Comparative Pathobiology, Purdue University, 625 Harrison St. West Lafayette, IN 47907

[b]Purdue University Center for Cancer Research, 201 S. University St. West Lafayette, IN 47907

[c]Department of Pharmacology and Toxicology & Department of Urology, Indiana University, 635 Barnhill Dr. Indianapolis, IN 46202

[d]School of Mechanical Engineering, Purdue University, 1205 W. State St. West Lafayette, IN 47907

[e]Birck Nanotechnology Center, Purdue University, 1205 W. State St. West Lafayette, IN 47907

[f]College of Veterinary Medicine, Purdue University, West Lafayette, Indiana; the Heeke Animal Disease Diagnostic Laboratory, 11367 East Purdue Farm Road Dubois, IN 47527

Abstract

Background—The presence of inflammation in prostate cancer (PCa) and benign prostate hyperplasia (BPH) has been well described but the cellular mechanisms by which inflammation modulates the prostate are currently unclear. Prostate stem cells (PSC) not only maintain prostate homeostasis but also are considered to be the cell of origin of PCa and an important contributor to BPH. However, the impact of inflammation on PSC is not well understood. Therefore, we initiated studies to evaluate the effect of inflammation on PSC.

Method—Ovalbumin specific $CD8^+$ T cells were intravenously delivered to intact and castrated prostate ovalbumin expressing transgenic-3 (POET-3) mice to induce inflammation. Lin (CD45/CD31)$^-$Sca1$^+$CD49f$^+$ cells (LSC) and progenitor cells within LSC were determined by flow cytometry. Sorted LSC were subjected to a prostate sphere forming assay to evaluate PSC clonal propagation, proliferation, immediate differentiation, and self-renewal ability. Density of individual spheres was measured by a cantilever-based resonator weighing system. Morphology and characterization of prostate spheres was determined by hematoxylin and eosin (H&E) staining and immunohistochemistry (IHC). Finally, immediate PSC differentiation in sphere formation was determined by immunofluorescence for epithelial cytokeratin markers cytokeratin (CK) 5 and CK8.

Result—Data presented here demonstrate a significant expansion of the proliferative ($BrdU^+$) LSC population, including $CK5^+$, $p63^+$, $CK18^+$ cells, as well as intermediate cells ($CK5^+/CK8^+$)

[1]Correspondence: Timothy L. Ratliff, Ph.D., Purdue University Center for Cancer Research, Hansen Life Sciences Research Building, 201 S. University St. West Lafayette, IN 47907-2064, Phone: 765-494-9129, tlratliff@purdue.edu.

in inflamed prostates. Histological images reveal that PSC from inflamed prostates produce significantly larger spheres, indicating that the enhanced proliferation observed in LSC is sustained *in vitro* in the absence of inflammatory mediators. In addition, cultures from inflamed PSC yielded increased number of tubule-like spheres. These tube-like spheres grown from PSCs isolated from inflamed mice exhibited stratification of a CK8+ luminal-like layer and a CK5+ basal-like layer. Notably, the numbers of spheres formed by inflamed and non-inflamed PSC were equal, suggesting that even though proliferation is enhanced by inflammation, the homeostatic level of PSC is maintained.

Conclusion—Induction of inflammation promotes PSC expansion and immediate differentiation through highly proliferative progenitor cells while the homeostasis of PSC is maintained.

Keywords

prostate stem cells; inflammation; prostate biology

Introduction

Prostate inflammation in association with the development of human benign prostate hyperplasia (BPH) and prostate carcinogenesis has been extensively discussed over last decades [1–4]. Imbalance of pro-inflammatory and anti-inflammatory cytokines, abnormal production of angiogenic and lymphangiogenic growth factors, and generation of reactive oxygen species from inflammatory infiltrates are considered among the potential initiators of prostatic malignancies [5, 6]. Epithelial prostate stem cells (PSC) have been regarded as the origin of hyper-proliferative epithelium and the main initiator of prostatic pathogenesis, and maybe the target of inflammatory compounds, which are also known to participate in neoplastic transformation [7]. However, little knowledge is available to link inflammatory modulation of PSC to BPH or prostate cancer. Understanding the impact of inflammation in regulating PSC will provide a foundation for future studies to define the relationship between prostate inflammation, BPH, and prostate cancer development.

Evidence of PSC restoration of prostate tissue was first demonstrated by castration followed by repeated cycles of androgen withdrawal-replenishment. Depletion of androgen as a result of castration led to involution of prostate epithelium, yet replenishment of androgen restored the prostate tissue due to resident stem cell proliferation and differentiation [8–10]. The impact of inflammation on adult stem cells has been observed in several organs. For example, hepatitis virus infection induced liver stem cells to replace damaged hepatocytes and choloangiocytes via cellular interactions between liver stem cells and adjacent inflammatory cells [11]. The impact of *E. coli*-induced inflammation on PSC was reported by Kwon and associates, who demonstrated that inflammation increased the conversion of basal PSC to luminal progenitors [12].

Cytokeratin (CK) profiles of human prostate glands, describing the difference among epithelial compartments, have been well-documented [13–16]. Basal cells with better cell plasticity display CK5, p63, and CK14 while functional luminal cells show expression of CK8 and CK18 [14]. Cells co-expressing basal and luminal CK markers were defined as intermediate cells, which appear during the prostate differentiation and regeneration

processes [16, 17]. The intermediate cells are regarded as an outcome of stem cell division. An enriched proliferative intermediate cell population was observed in human proliferative inflammatory atrophy (PIA) prostate specimens [18]. In addition, p63, a homolog of the p53 tumor suppressor gene and critical stem cell proliferation regulator in epithelial development, is upregulated in *E-coli* challenged murine prostates [19–21]. Histological data of intermediate cells listed above indicate that the multipotent and self-renewable PSC might be modulated by inflammation, though further evidence is required.

Here we present a T cell mediated prostatitis mouse model, prostate ovalbumin expressing transgenic-3 mouse model (POET-3), in which ovalbumin (OVA) expression is driven by a composite probasin promoter (ARR_2PB) [22], to mimic antigen specific autoimmunity and pathological outcomes of human chronic prostatitis. The data obtained from studies in the POET-3 inflammation model demonstrated a sustained epithelial cell hyper-proliferation, significantly elevated cytokine/chemokine protein expression, and strong infiltration of leukocytes after adoptive transfer of $CD8^+$ cytotoxic T cells [3]. To enrich the murine PSC population in POET-3 mice, we adopted an established marker system in identification of prostate progenitors: stem cell antigen-1 (Sca-1) and integrin-α6 (CD49f) [23]. Lin (CD45/CD31)$^-$Sca1$^+$CD49f$^+$ (LSC) cells were reported to generate a 60-fold enrichment for prostate sphere forming capacity *in vitro* and were able to form a prostate graft *in vivo* [24]. PSC within the murine LSC population were functionally identified via the prostate sphere forming assay in which one stem cell generates a single sphere [25]. The combination of the POET-3 model and the well-established strategy for accessing PSC allows us to understand the biology of inflammation regulated PSC. Data presented here show that OVA-specific $CD8^+$ T-cell challenged prostates display increased LSC, in which increased numbers of $CK5^+$, $p63^+$, and $CK18^+$ cells are also detected. The entire process is independent from the presence of androgen, suggesting the outcome of an increased progenitor population is solely regulated by the inflammatory environment. Given the increased amount of proliferative prostate progenitor cells in inflamed prostates, the sustained ratio of PSC within LSC suggests that the homeostasis of PSC is not altered by induction of inflammation while the proliferation rate of daughter progenitor cells derived from inflamed PSC is strongly elevated. Higher percentage of tubule-like spheres in the inflamed setting was identified by two-dimensional H&E stained histological sections and a three-dimensional single cell weighing system. Inflamed spheres revealed a significantly higher density compared to average mammalian cell density, which is approximate to the value of protein density, indicating inflammation regulated PSC are able to generate more protein secreting daughter cells, likely a more committed progenitor population.

Materials and Methods

Mice

Prostate ovalbumin expressing transgenic-3 mice (POET-3, C57BL/6 background) were generated as previous described [6, 26, 27]. In summary, Rag1$^{-/-}$Thy1.1$^+$OTI mice were generated by breeding C57BL/6 Thy1.1$^+$ mice (Jackson Laboratories) with Rag1$^{-/-}$ mice (a gift from Dr. W.E. Heath, The Walter and Eliza Hall Institute of Medical Research, Melbourne, Australia). All animals were housed and maintained under pathogen free

conditions with 12 hour-light/12 hour-dark cycles. Orchiectomy was performed on POET-3 mice at age 8–12 weeks. All procedures involving mouse welfare have conformed to national rules and Purdue Animal Use and Committee (PACUC) approved protocols (1112000137).

Induction of inflammation

Splenocytes were isolated from $Rag1^{-/-}Thy1.1^{+}$OTI mice, activated by 1μg/mL SIINFEKL (Ova peptide 257–264, Cat#.74-1-16B, American Peptide) for 48 hours *in vitro*. Activated $Thy1.1^{+}CD8^{+}$ T cells were collected and purified by Ficol (Atlanta Biologicals). 5×10^{6} purified OT-I cells were later transferred into POET-3 mice intravenously to induce inflammation. OT-I cells injected mice and naïve POET-3 mice were raised for another 6 days and prostate tissues were harvested for further processing.

Isolation of LSC population

Prostate epithelial cells were isolated from 8–12 week old naïve and inflamed POET-3 mice. The procedure for isolation prostate progenitor population was followed from a published protocol [23]. Briefly, we digested minced prostate tissue with 1mg/mL collagenase-I (Cat#. 5138, Sigma-Aldrich) in RPMI1640 containing 10% fetal bovine serum (FBS) for 2 hours, following trypsinization at 37 °C to release mice prostate cells from tissue. Prostate epithelial cells were passed through 20G needles 3–5 times and 40μm cell strainers to eliminate aggregates. To enrich prostate progenitor population, isolated cells were incubated with fluorescence conjugated specific antibodies: Sca1-APC (Cat#.108112, BioLegend), CD49f-PE (Cat#.12-0495-83, eBioscience), CD45-FITC (Cat#.103108, BioLegend), and CD31-FITC (Cat#.553372, BD Bioscience). $CD45^{-}CD31^{-}Sca1^{+}CD49f^{+}$ (annotated as $Lin^{-}Sca1^{+}CD49f^{+}$, LSC population in this article) live cell sorting was performed on the BD FACS Aria in sterile condition.

Flow cytometry analysis

Prostate tissues were processed as describe above. Single cell suspensions from naïve and inflamed prostates were stained with fluorescence conjugated antibodies: Sca1-APC, CD49f-PE, and CD45-Percp, for 20 mins at 4 °C, stained cells were then fixed in 10% neutral buffered formalin (NBF). To identify transit-amplifying cells and proliferative basal cells in LSC population, 10%NBF fixed sample were stained with unconjugated antibodies: CK5 (Cat#.MAB3228, Millipore, 1:100), p63 (Cat#.sc8431, Santa Cruz, 1:100), and CK18 (Cat#.ab668, Abcam, 1:100), following secondary Alexa 488 (Invitrogen, 1:500) by using BD Pharmagin cell staining kit. BrdU staining was done by FITC BrdU flow kit (Cat#. 51-2354AK, BD Pharmingen). Flow cytometry analyses were performed at BD FACS Canto II.

RNA Isolation and Quantitative Gene Expression Analysis

Total RNA was isolated from intact POET-3, castrated POET-3, and C57BL/6J mouse prostates using OMEGA E.Z.N.A Total RNA kit and cDNA was generated using PerfecTa®qPCR FastMix® II (Quanta Bioscience). Quantitative real-time polymerase chain reaction (qRT-PCR) was carried out by OVA primer sets:

AATGAGCATGTTGGTGCTGTTGC, GAAACACATCTGCCAAAGAAGAGAACG, and 18S control (IDT) along with FastStart Universal SYBR Green Master (Cat#. 04913850001, Roche) on LightCycler® 96 instrument (Roche). The mean of triplicates was derived from 3 independent mice in each group.

Prostate sphere forming assay

Sorted LSC population was re-suspended in 2:1 Matrigel/Prostate Epithelial growth medium (Matrigel, Cat#.354234, Corning; PrEGM, Cat#.CC-3166, Lonza) in a total volume of 120μL. Cells were seeded at a density of 8,000 or 10,000 cells per well in 12-well plates, and incubated for 7 days. Half medium change was performed every 2–3 days. Numbers of spheres were counted manually at 40x magnification at 7th day under microscope. To examine self-renewal ability of PSCs, spheres from primary culture were released by 1mg/mL Dispase (Cat#.17105-041, Invitrogen) at 37 °C for an hour, and dissociated into single cells for secondary sphere culture. To dissociate intact spheres, collected spheres were incubated with trypsin at room temperature (R.T.) for 10 mins. Trypsinized cells from spheres were passed through 26G needles three times. Dissociated cells were individually plated at 8,000 cells per well density in 12-well plates for 7 days. The numbers of secondary spheres were obtained at 7th day.

Histology analysis

To analyze the morphology and identify phenotypes of spheres, intact spheres released from Matrigel were fixed in 10% NBF for an hour, following dehydration by incubating in 70% ethanol for another hour. All fixed spheres were embedded in histogel and then in paraffin, sectioned, and processed for Hematoxylin and Eosin (H&E) staining and immunohistochemistry. Percentages of different morphological spheres were identified by H&E stained slides. Total number of two types of spheres was collected from 3–4 independent experiments. Fisher's test was applied in the analysis of contingency tables (Table. 1). Immunofluorescence (IF) and DAB-immunohistochemistry (IHC) were performed as previously described [28, 29]. Primary antibodies for IF includes: rabbit anti-cytokeratin 5 (1:100, Biolegend), mouse anti-p63 (1:50, Biocare Medical) and mouse anti-cytokeratin 8 (1:100, Novus). Secondary Alexa 488 or Alexa 594 were conjugated for 1 hour at room temperature (1:100, Invitrogen), followed by 10 minutes incubation with Hoechst 33258 to visualize the nuclei (1μg/ml). Sphere sections were washed and covered with an aqueous medium and glass coverslips. The sections were photographed and analyzed by immunofluorescence and the number of positive- and negative-stained cells was determined. Primary antibody for IHC is rabbit anti-Ki67 (1:100, Abcam) was utilized for primary detection. Freshly sorted LSC was span down onto slides at 800rpm for 3 mins, and fixed with 4% paraformaldehyde. Primary antibodies include: rabbit anti-cytokeratin 5 (1:100, Biolegend), and mouse anti-cytokeratin 8 (1:100, Novus). Secondary Alexa 488 or Alexa 594 were conjugated for 1 hour at room temperature (1:500, Invitrogen). Representative images were determined by at least 3 animals per group.

Measurement of sphere size and density

To measure diameters of spheres, images of individual H&E stained spheres were taken at 400x magnifications under microscopy. Spheres were manually circled using Image J and

Feret diameters were obtained via software calculation. Paraformaldehyde-fixed spheres were first air-dried on a glass slide. Individual spheres were picked up by a micromanipulator under a microscope [30] and placed on a cantilever-based resonator for weighing. The experimental configurations and measurement principles pertaining to mass detection were listed in a previous study [31]. The effective density of the loaded prostate sphere was calculated by dividing the measured mass by the effective volume calculated based on microscopic observation.

Statistical analysis

Statistical analyses were performed on Prism (Version 5.04). Student's t-test was utilized for most of comparisons between naïve and inflamed groups, except that Fisher's test was utilized for comparing the ratio of solid and tubule-like spheres. Statistical significance was determined by $p<0.05$.

Results

Induction of inflammation promotes prostate progenitor cell proliferation

To test whether inflammation increases the number of prostate progenitor cells, we determined the number of prostate cells expressing various markers in inflamed POET-3 mice. Flow cytometry analysis of the inflamed prostates showed induction of a strong inflammatory response. CD45 positive cells represented the total leukocyte population in prostates, whereas Sca1 and CD49f labeled the prostate progenitor population, namely the Lin $(CD45/CD31)^{-}Sca1^{+}CD49f^{+}$ (LSC) population, within the non-leukocytic cell population [23, 24].

Compared to naïve prostates, inflamed prostates contained a 20-fold increase in the number of CD45-positive cells, indicating that the induction of inflammation significantly expanded the total leukocyte population in prostates (Fig. 1A). A previous study defined the composition of recruited leukocytes, including endogenous $CD4^{+}$, $CD8^{+}$ T-cells, $Foxp3^{+}CD4^{+}$ regulatory T-cells, and $Gr\text{-}1^{+}CD11b^{+}$ myeloid derived suppressive cells [3]. Leukocyte expansion resulted in 2.7-fold increase in the LSC population (Fig. 1B). Absolute numbers of LSC in inflamed prostates were significantly higher than those in naïve setting (*p<0.0001*) (Fig. 1C).

To understand the source of these extra cells, we asked whether inflammation increases cell proliferation. In inflamed LSC, more BrdU-positive cells were detected (*p=0.0026*), suggesting that cell proliferation was a contributing factor to the cell number increase (Fig. 1D). To further profile the progenitor components, we examined the expression level of CK5, p63, and CK18 within LSC. Intracellular staining of individual marker along with LSC surface labeling allowed observation of the distribution of different cell types within LSC. Significantly, the number of $CK5^{+}$ (Fig. 1E), $p63^{+}$ (Fig. 1F), and $CK18^{+}$ (Fig. 1G) cells within LSC were increased in inflamed prostates. Immunofluorescence staining shows that $CK5^{+}/CK8^{+}$ co-expressing cells, namely the intermediate progenitor cells, are exhibited in inflamed LSC, while $CK8^{+}$ cells are barely detected in naïve LSC (Fig. 2).

Inflammation-driven PSC expansion is independent of testicular androgen

Androgen has been considered as a main contributor of prostate epithelial restoration in rodents [8–10]. To clarify whether the increased number of LSC (as a consequence of PSC expansion), was a net result of inflammation, we castrated POET-3 mice to deplete circulating androgen and subsequently induced prostate inflammation. Two weeks after orchiectomy, expression of OVA is detected in castrated animals by qRT-PCR, in which the expression level is similar to intact animals (Fig. 3A). Hence, OT-I cells were delivered to induce inflammation and murine prostates were harvested 6 days after OT-I delivery (Fig. 3B). In the castrated OTI treated POET-3 mice, a significant increase in LSC was observed in comparison to castrated POET-3 mice not receiving OT-I cells ($p=0.015$) (Fig. 3C, and D). These data demonstrate that inflammation-driven PSC expansion did not require testicular androgen.

Inflammation regulated PSC give rise to larger spheres with a more tubule-like feature

Given the increased amount of prostate progenitor cells *in vivo*, we hypothesize that PSC are more proliferative. We examined the size of clonally formed prostate spheres by identifying diameters in two-dimensional hematoxylin and eosin (H&E) stained sections (Fig. 4A). As a result, PSC from inflamed prostates clonally generated larger spheres (both solid and tubule-like) in term of diameters (Fig. 4B). In addition, the inflamed spheres show a significantly higher percentage of tubule-like spheres in H&E stained sections (41% in inflamed versus 21% in naïve spheres, Fisher's test, $p=0.0035$) (Table. 1).

To further investigate the physical composition of the two types, we weighed the biomass of individual spheres by cantilever based resonator to identify the effective density of spheres (Fig. 4C) [30, 32]. Inflamed spheres showed an average density of 1.29 g/cm^3, which was more similar to the density of protein (1.22–1.43 g/cm^3) than to the density of mammalian cells (1.04–1.1 g/cm^3) [33]. Comparatively, the mean of the density curve in naïve spheres fell at 1.1 g/cm^3, which was significantly different from the mean of inflamed spheres ($p<0.0001$) (Fig. 4D). This result suggests that inflammation enabled PSC to generate more tubule-like spheres, which may consist of more protein secreting daughter cells.

The homeostasis of PSC maintained after induction of inflammation

Each prostate sphere was clonally derived from a single stem cell; therefore, the number of spheres indicated the number of true stem cells within LSC. No difference in the number of first generation spheres was observed between naïve and inflamed prostates when a fixed number of LSC were seeded, indicating that the ratio of PSC within the LSC population was maintained at its normal homeostatic level in the presence of inflammation (Fig. 5A). In addition, no difference in self-renewal ability was determined between naïve and inflamed groups by secondary passage of dissociated spheroid cells (Fig. 5B).

The organized structures of prostate spheres with lineage hierarchy was determined previously [25]. Here we adopted the same strategy to determine morphologies of prostate spheres derived from inflammation regulated PSC. Spheres from inflamed prostates reveal a similar lineage hierarchy compared to naïve spheres, in which both basal (CK5) and luminal (CK8) cells are better stratified within spheres, with CK8 signal is stronger in the center.

Both proliferative progenitor cells ($Ki67^+$) and highly self-renewable ($p63^+$) cells are detected in the edge of spheres (Fig. 5C). The average number of $Ki67^+$ and $p63^+$ cells per sphere is higher in inflamed group (Fig. 5D and E), though the ratio of $Ki67^+$and highly self-renewable $p63^+$ to total cell number shows no difference between naïve and inflamed groups (Fig. 5F and G).

Discussion

Pathological evidence has shown a link between prostate inflammation and prostate cancer. For example, instances of prostate inflammatory atrophy (PIA) lesions directly merging with cancer were identified in 14 of 50 (28%) patient specimens [34]. Likewise, studies in POET-3/$PTEN^{+/-}$ mice showed the development of inflammation and occurrence of PIA four months after induction of inflammation [29]. PIA was defined as a regenerative lesion by showing elevated anti-apoptotic factor (Bcl-2), as well as many proliferative cells (Ki67) within atrophic lesions, where no obvious tissue destruction was determined, possibly due to prostate epithelial repopulation [3, 26, 35]. Data presented in this manuscript address phenomena associated with the acute inflammatory process (day 6 after induction) and do not address regenerative processes like PIA. However, there is very little appreciation of the cellular mechanisms involved in such regenerative modulation of prostate epithelium during inflammation due to the lack of a representative animal model. While the *E. coli* induced inflammation model is an extensively utilized model for studying prostate inflammation, bacterial prostatitis is a relatively rare condition, occurring in only approximately 5% of prostatitis cases [36]. The majority of prostatitis patients present with non-bacterial inflammatory condition that is hypothesized to be autoimmune in nature [36, 37]. Our laboratory has established a prostate specific autoimmune prostatitis mouse model, POET-3, in which a strong recruitment of $CD4^+$, $CD8^+$ T-cells, and $CD4^+Foxp3^+$ T-reg cells; elevated cytokine/chemokine expression; as well as sustained prostate epithelial hyper-proliferation, were identified [6].

OVA expression in murine prostate is driven by an androgen sensitive promoter (ARR_2PB) [38, 39]. Our data suggest that OVA expression is similar between intact and castrated animals, which is possibly due to the presence of other sources of androgen in castrated animals, for example, adrenal androgen and *de novo* synthesized androgen [40]. Hence OVA expression in castrated POET-3 mice is still sufficient to induce inflammation [38, 41]. Given that, the magnitude of LSC increase in testicular androgen depleted mice is exactly the same as in intact mice, the data suggest that inflammation driven PSC expansion does not require the presence of testicular androgen, which normally is the main trigger for expanding prostate epithelium [42]. Additionally, inflammation enhanced the stromal population ($Lin^-Sca1^+CD49f^-$) [24] in POET-3 mice prostates. The role of stromal cells in chronic inflammatory niche is to maintain leukocyte accumulation by sequentially expressing adhesion molecules and chemokines/cytokines [43]. The inflammatory chemokine/cytokine elicited signal transductions can further affect epithelial turnover through stromal cells. For instance, interleukin-6 (IL-6) family induced Jak-Stat3 pathway up-regulates paracrine Wnt signaling can either maintain stemness property of stem cells, or enhance local mature cell proliferation [44]. Therefore, the impact of the enhanced stromal population on promoting PSC proliferation will be an interesting focus for future studies.

Asymmetrical basal-origin PSC expansion was determined in previous studies [45, 46]. Flow cytometry analysis of prostate progenitor cells shows a net outcome of PSC expansion, while the *in vitro* sphere forming assay enables one to evaluate asymmetrical cell division as a process of PSC self-renewal and propagation of daughter progenitor cells. By plating a fixed number of cells from inflamed and naïve prostate tissue, the ratio of true PSC can be assessed by evaluating the number of spheres that form. The fixed ratio of first and secondary sphere formation revealed that sphere formation was equivalent between inflamed and naïve cultures, indicating that PSC homeostasis was maintained in inflamed prostates. In addition, the fixed ratio of Ki-67$^+$ and p63$^+$ cells within different sizes of spheres corroborates the maintenance of homeostasis. The presence of larger spheres in cultures derived from inflamed prostate tissue suggests that inflammation induces a change in PSC that is maintained in the absence of both inflammatory mediators and androgen in the *in vitro* cultures. These data suggest that the *in vivo* induction of inflammation promoted PSC asymmetrical division, where self-renewal of PSC is maintained and their progenitor daughter cells are more proliferative.

Two types of clonally derived prostate spheres, solid and tubule-like spheres, have been commonly reported in previous studies [23, 25]. Our data showed that cross-sections of tubule-like spheres were better stratified with basal (CK5) to luminal (CK8) hierarchy and showed canalized lumens filling with secretory materials. Nevertheless, the distinct morphology of both types of spheres has never been fully addressed as a biological outcome in PSC derived spheres. Here we determined that inflammation regulated PSC generated a higher percentage of tubule-like spheres, which included secretory proteins, as suggested by Eosin staining of the luminal material and the demonstration of distinct effective densities between solid and tubule-like spheres. A recent study in bacterial prostatitis also demonstrated a basal-to-luminal differentiation of prostate epithelial cells in response to inflammation [12], which supported our observation that inflammation modulated PSC were committed to a more differentiated progenitor phenotype, the tubule-like spheres.

In addition, even though inflammatory mediators were absent during culture, significantly different sphere sizes and ratio of two types of spheres between naïve and inflamed groups were observed. Preliminary data demonstrates that the diameters of both first and second generation inflamed spheres are similar (119.7 ± 5.74 vs 122.9 ± 13.48, respectively; Mean ± SE), which both are significantly larger than their counterpart naïve spheres. In other words, the impact of inflammation on PSC remained and lasted after removal from the inflammatory milieu for two generations. One possibility for why this may have occurred is that epigenetics modulation of gene expression is involved. An epigenetic switch on cellular transformation was rigorously demonstrated by Struhl's group in 2009. The inflammatory circuit, including NF-κB, IL-6, Lin28b, and miRNA let-7a, allowed naïve mammalian cells to adopt and maintain transformed phenotypes after removal of oncogenic stimulation [47]. Therefore it is possible that PSC go through a certain epigenetic switch upon the acute induction of inflammation *in vivo*.

Conclusion

Utilizing the POET-3 model, we present phenotypic and functional evidence of PSC expansion upon the induction of T-cell mediated autoimmune inflammation. Active PSC cell division, as a result of induction of inflammation, reveals an asymmetrical pattern, in which the rate of PSC self-renew is maintained while the proliferation rate of generating daughter progenitor cells is highly enhanced.

Acknowledgments

We thank Dr. Jill Hutchcroft at Purdue Flow Cytometry & Cell Separation Facility for cell sorting; Tracy Wiegand, and Carol Bain at Purdue Histology & Phenotyping Laboratory for sphere sectioning and H&E staining; and Cansu Cimen Bozkus for manuscript proofreading. This work was supported by NIDDK 2R01DK084454-05 and Purdue Center of Cancer Research P30 CA023168.

References

1. Bastian PJ, et al. Molecular biomarker in prostate cancer: the role of CpG island hypermethylation. Eur Urol. 2004; 46(6):698–708. [PubMed: 15548435]
2. De Marzo AM, Nakai Y, Nelson WG. Inflammation, atrophy, and prostate carcinogenesis. Urol Oncol. 2007; 25(5):398–400. [PubMed: 17826659]
3. Haverkamp JM, et al. An inducible model of abacterial prostatitis induces antigen specific inflammatory and proliferative changes in the murine prostate. Prostate. 2011; 71(11):1139–50. [PubMed: 21656824]
4. Sfanos KS, De Marzo AM. Prostate cancer and inflammation: the evidence. Histopathology. 2012; 60(1):199–215. [PubMed: 22212087]
5. Coussens LM, Werb Z. Inflammation and cancer. Nature. 2002; 420(6917):860–7. [PubMed: 12490959]
6. Haverkamp J, Charbonneau B, Ratliff TL. Prostate inflammation and its potential impact on prostate cancer: a current review. J Cell Biochem. 2008; 103(5):1344–53. [PubMed: 17955503]
7. Goldstein AS, et al. Identification of a cell of origin for human prostate cancer. Science. 2010; 329(5991):568–71. [PubMed: 20671189]
8. English HF, Santen RJ, Isaacs JT. Response of glandular versus basal rat ventral prostatic epithelial cells to androgen withdrawal and replacement. Prostate. 1987; 11(3):229–42. [PubMed: 3684783]
9. Isaacs JT, Coffey DS. Etiology and disease process of benign prostatic hyperplasia. Prostate Suppl. 1989; 2:33–50. [PubMed: 2482772]
10. Isaacs JT. Prostate stem cells and benign prostatic hyperplasia. Prostate. 2008; 68(9):1025–34. [PubMed: 18386293]
11. Sun B, Karin M. Inflammation and liver tumorigenesis. Front Med. 2013; 7(2):242–54. [PubMed: 23681888]
12. Kwon OJ, et al. Prostatic inflammation enhances basal-to-luminal differentiation and accelerates initiation of prostate cancer with a basal cell origin. Proc Natl Acad Sci U S A. 2014; 111(5):E592–600. [PubMed: 24367088]
13. Nagle RB, et al. Cytokeratin characterization of human prostatic carcinoma and its derived cell lines. Cancer Res. 1987; 47(1):281–6. [PubMed: 2431765]
14. Verhagen AP, et al. Colocalization of basal and luminal cell-type cytokeratins in human prostate cancer. Cancer Res. 1992; 52(22):6182–7. [PubMed: 1384957]
15. Sherwood ER, et al. Differential cytokeratin expression in normal, hyperplastic and malignant epithelial cells from human prostate. J Urol. 1990; 143(1):167–71. [PubMed: 1688457]
16. Verhagen AP, et al. Differential expression of keratins in the basal and luminal compartments of rat prostatic epithelium during degeneration and regeneration. Prostate. 1988; 13(1):25–38. [PubMed: 2458583]

17. Hudson DL, et al. Epithelial cell differentiation pathways in the human prostate: identification of intermediate phenotypes by keratin expression. J Histochem Cytochem. 2001; 49(2):271–8. [PubMed: 11156695]
18. van Leenders GJ, et al. Intermediate cells in human prostate epithelium are enriched in proliferative inflammatory atrophy. Am J Pathol. 2003; 162(5):1529–37. [PubMed: 12707036]
19. Senoo M, et al. p63 Is essential for the proliferative potential of stem cells in stratified epithelia. Cell. 2007; 129(3):523–36. [PubMed: 17482546]
20. Pignon JC, et al. p63-expressing cells are the stem cells of developing prostate, bladder, and colorectal epithelia. Proc Natl Acad Sci U S A. 2013; 110(20):8105–10. [PubMed: 23620512]
21. Khalili M, et al. Loss of Nkx3.1 expression in bacterial prostatitis: a potential link between inflammation and neoplasia. Am J Pathol. 2010; 176(5):2259–68. [PubMed: 20363913]
22. Zhang JF, et al. A small composite probasin promoter confers high levels of prostate-specific gene expression through regulation by androgens and glucocorticoids in vitro and in vivo. Endocrinology. 2000; 141(12):4698–4710. [PubMed: 11108285]
23. Lukacs RU, et al. Isolation, cultivation and characterization of adult murine prostate stem cells. Nat Protoc. 2010; 5(4):702–13. [PubMed: 20360765]
24. Lawson DA, et al. Isolation and functional characterization of murine prostate stem cells. Proc Natl Acad Sci U S A. 2007; 104(1):181–6. [PubMed: 17185413]
25. Xin L, et al. Self-renewal and multilineage differentiation in vitro from murine prostate stem cells. Stem Cells. 2007; 25(11):2760–9. [PubMed: 17641240]
26. Lees JR, et al. T-cell recognition of a prostate specific antigen is not sufficient to induce prostate tissue destruction. Prostate. 2006; 66(6):578–90. [PubMed: 16388504]
27. Lees JR, et al. Deletion is neither sufficient nor necessary for the induction of peripheral tolerance in mature CD8+ T cells. Immunology. 2006; 117(2):248–61. [PubMed: 16423061]
28. Hahn AM, et al. Interleukin-driven insulin-like growth factor promotes prostatic inflammatory hyperplasia. J Pharmacol Exp Ther. 2014; 351(3):605–15. [PubMed: 25292180]
29. Burcham GN, et al. Impact of prostate inflammation on lesion development in the POET3(+)Pten(+/−) mouse model of prostate carcinogenesis. Am J Pathol. 2014; 184(12):3176–91. [PubMed: 25455686]
30. Chan BD, et al. A Compact Manually Actuated Micromanipulator. Journal of Microelectromechanical Systems. 2012; 21(1):7–9.
31. Chan BD, et al. Selective Weighing of Individual Microparticles Using a Hybrid Micromanipulator-Nanomechanical Resonator System. Ieee Sensors Journal. 2013; 13(8):2857–2862.
32. Chan BD, et al. On-demand weighing of single dry biological particles over a 5-order-of-magnitude dynamic range. Lab Chip. 2014; 14(21):4188–96. [PubMed: 25162712]
33. Fischer H, Polikarpov I, Craievich AF. Average protein density is a molecular-weight-dependent function. Protein Sci. 2004; 13(10):2825–8. [PubMed: 15388866]
34. Wang W, Bergh A, Damber JE. Morphological transition of proliferative inflammatory atrophy to high-grade intraepithelial neoplasia and cancer in human prostate. Prostate. 2009; 69(13):1378–86. [PubMed: 19507201]
35. De Marzo AM, et al. Proliferative inflammatory atrophy of the prostate: implications for prostatic carcinogenesis. Am J Pathol. 1999; 155(6):1985–92. [PubMed: 10595928]
36. Habermacher GM, Chason JT, Schaeffer AJ. Prostatitis/chronic pelvic pain syndrome. Annu Rev Med. 2006; 57:195–206. [PubMed: 16409145]
37. Motrich RD, et al. Presence of INFgamma-secreting lymphocytes specific to prostate antigens in a group of chronic prostatitis patients. Clin Immunol. 2005; 116(2):149–57. [PubMed: 15993362]
38. Zhang J, et al. A small composite probasin promoter confers high levels of prostate-specific gene expression through regulation by androgens and glucocorticoids in vitro and in vivo. Endocrinology. 2000; 141(12):4698–710. [PubMed: 11108285]
39. Kurts C, et al. Constitutive class I-restricted exogenous presentation of self antigens in vivo. J Exp Med. 1996; 184(3):923–30. [PubMed: 9064352]

40. Mohler JL. Concept and viability of androgen annihilation for advanced prostate cancer. Cancer. 2014; 120(17):2628–37. [PubMed: 24771515]
41. Sykulev Y, et al. Evidence that a single peptide-MHC complex on a target cell can elicit a cytolytic T cell response. Immunity. 1996; 4(6):565–71. [PubMed: 8673703]
42. Matusik RJ, et al. Prostate epithelial cell fate. Differentiation. 2008; 76(6):682–98. [PubMed: 18462434]
43. Naylor AJ, Filer A, Buckley CD. The role of stromal cells in the persistence of chronic inflammation. Clin Exp Immunol. 2013; 171(1):30–5. [PubMed: 23199320]
44. Katoh M. STAT3-induced WNT5A signaling loop in embryonic stem cells, adult normal tissues, chronic persistent inflammation, rheumatoid arthritis and cancer (Review). Int J Mol Med. 2007; 19(2):273–8. [PubMed: 17203201]
45. Wang J, et al. Symmetrical and asymmetrical division analysis provides evidence for a hierarchy of prostate epithelial cell lineages. Nat Commun. 2014; 5:4758. [PubMed: 25163637]
46. Polson ES, et al. Monoallelic expression of TMPRSS2/ERG in prostate cancer stem cells. Nat Commun. 2013; 4:1623. [PubMed: 23535644]
47. Iliopoulos D, Hirsch HA, Struhl K. An epigenetic switch involving NF-kappaB, Lin28, Let-7 MicroRNA, and IL6 links inflammation to cell transformation. Cell. 2009; 139(4):693–706. [PubMed: 19878981]

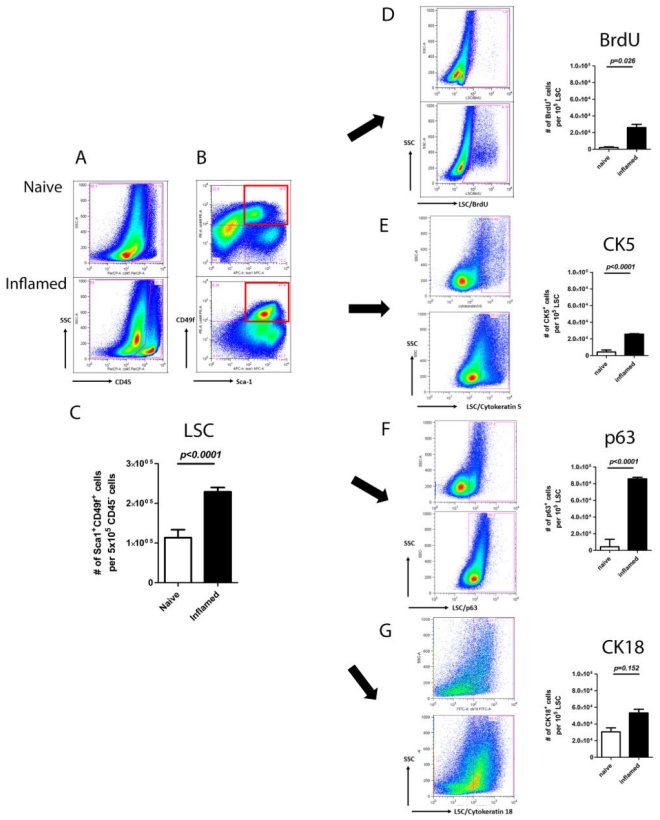

Fig. 1.

Induction of inflammation results in elevated prostate progenitor population. In this figure, the FACS plots of naïve and inflamed settings show on the upper and lower rows respectively: **(A)** $CD45^+$ cells. **(B)** $CD45^-Sca1^+CD49f^+$ cell (LSC) populations. Red squares gate out LSC population of progenitor cell marker analysis. **(C)** Bar graph of LSC in naïve and inflamed prostates. **(D)** $BrdU^+$ **(E)** $CK5^+$ **(F)** $p63^+$ **(G)** $CK18^+$ cells within LSC population. Bar graphs of different marker expressions are shown along with the corresponding FACS plots. (Student's t-test was determined by n=2–12 animals each group; error bar=SE.)

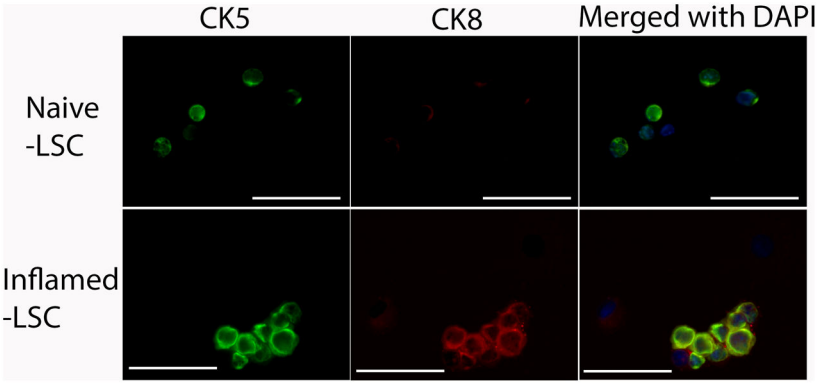

Fig. 2.

Representative IF images show the heterogeneity of LSC population in naïve and inflamed LSC, in which inflamed LSC reveals intermediate progenitor cells (CK5 and CK8 co-expressing cells). The upper panel shows $CK5^+$ cells (green), no $CK8^+$ cells (red), as well as $CK5^-/CK8^-$ cells in naïve LSC. The lower panel shows $CK5^+$ (green), $CK5^+/CK8^+$ (green/red) co-expressing cells, as well as $CK5^-/CK8^-$ cells in inflamed LSC. (Scale bar: 50 μm)

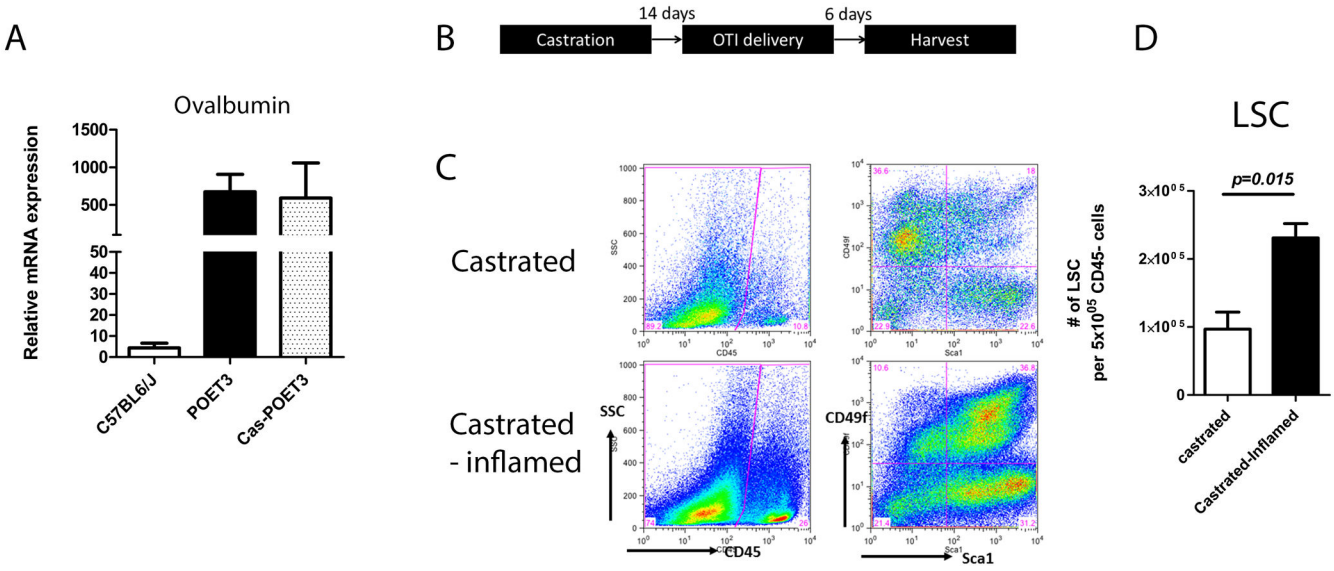

Fig. 3.

Inflammation driven prostate progenitor expansion is testicular-androgen independent. **(A)** Relative mRNA expression of OVA in intact and castrated POET-3 mice. Values of relative mRNA expression were means ± SE for n=3 per group. **(B)** Scheme summarizing experimental time frame of inflammation on castrated mice. **(C)** FACS plot of infiltrated $CD45^+$ cells (left panel) and LSC population (right panel) in castrated mice, with and without induction of inflammation. **(D)** Bar graphs of LSC in androgen depleted non-inflamed and inflamed prostates. (Student's t-test was determined by n=3 animals each group; error bar=SE.)

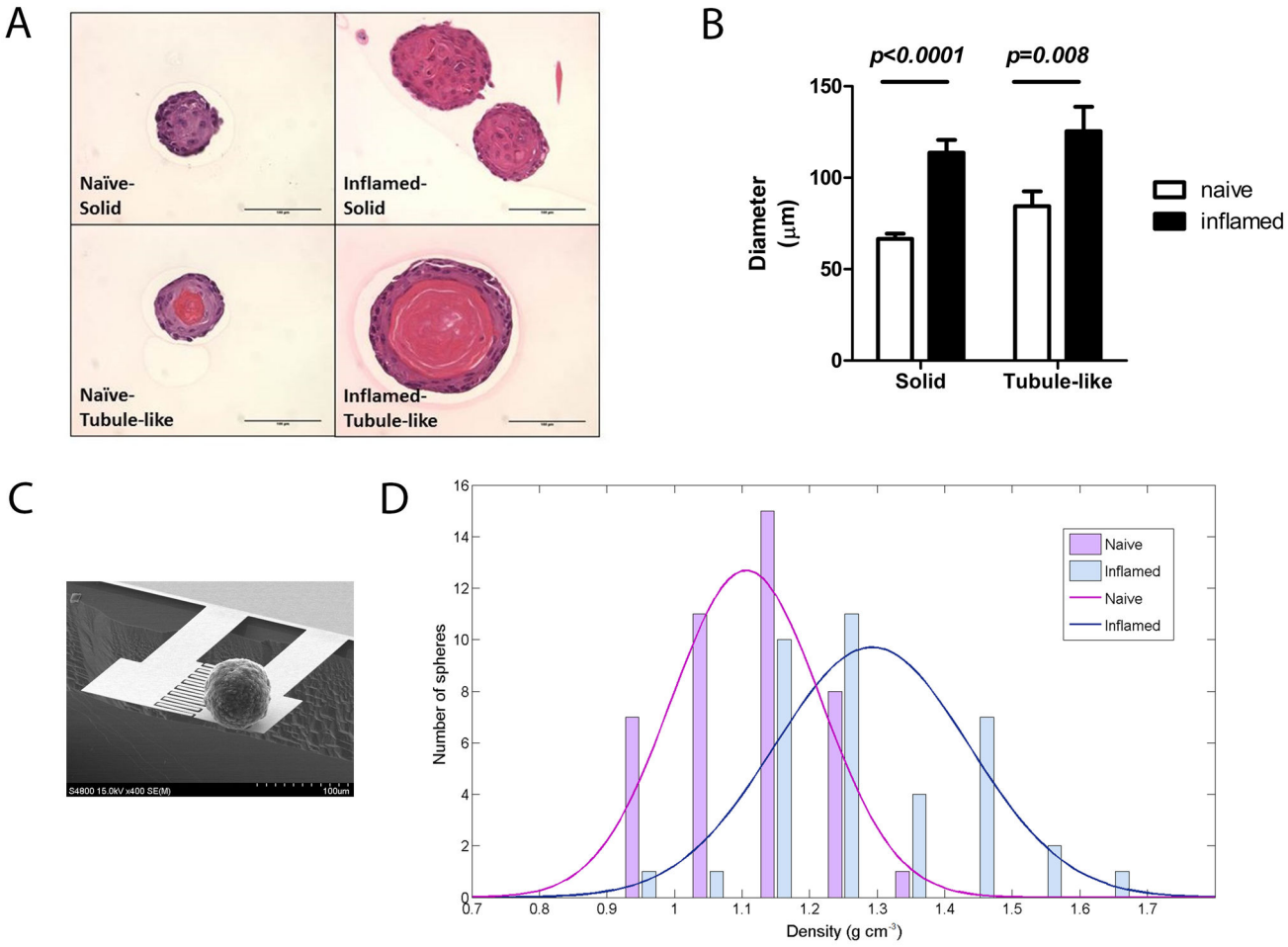

Fig. 4.

Inflammation regulated PSC generates larger spheres, as well as more tubule-like spheres. **(A)** H&E stained sections showed solid spheres (upper) and tubule-like spheres (lower) in naïve and inflamed groups. (Scale bar: 100 μm) **(B)** A bar graph shows diameters of two types of spheres. (n=46 in naïve solid spheres; n=12 in naïve tubule-like spheres; n=17 in inflamed solid spheres; n=12 in inflamed tubule-like spheres; error bar=SE; determinations were combined from 3 independent experiments.) **(C)** A scanning electron microscope (SEM) image shows weighing of an inflamed prostate sphere. The resonator comprised a sensor and a reference cantilever beam. **(D)** The average density of inflamed spheres (blue bars and curve) is 1.29 g/cm^3; naïve spheres (red bars and curve) is 1.1 g/cm^3. Specific values of density on x-axis correspond to the actual numbers of spheres on y-axis. (n=42 in naïve group; n=37 in inflamed group; Student's t-test, p<0.0001)

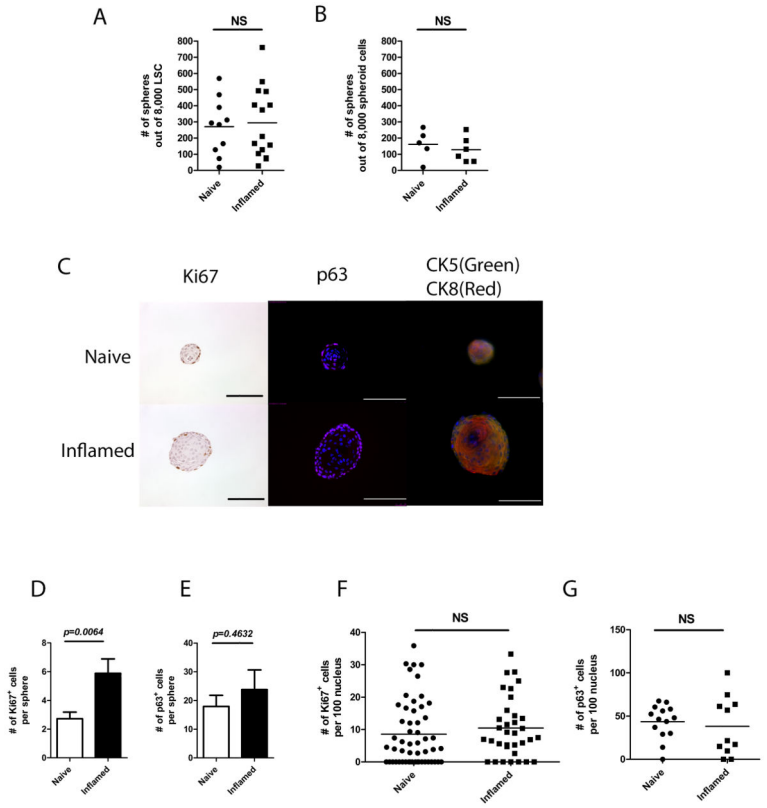

Fig. 5.

The ratio of PSC within LSC population is maintained. **(A)** A dot graph shows the number of first generation spheres derived from naïve and inflamed LSC. (5 separate experiments in naïve group and 7 in inflamed group, each experiment is presented in duplicates; Student's t-test, *p=0.87*) **(B)** A dot graph shows the number of secondary spheres derived from first generation spheres in naïve and inflamed settings. (3 separate experiments, each experiment was presented in duplicates; Student's t-test, *p=0.89*) **(C)** Histological images show Ki67, p63, and CK5/CK8 staining of spheres from naïve and inflamed prostates. (Scale bar: 100μm) **(D)** A bar graph shows the number of $Ki67^+$ cells per sphere. **(E)** A bar graph shows the number of $p63^+$ cells per sphere. **(F)** A dot graph shows the ratio of $Ki67^+$ cells within 100 sphere cells. **(G)** A dot graph shows the ratio of $p63^+$ cells within 100 sphere cells. (For Ki67 staining, n=54 in naïve spheres; n=34 in inflamed spheres; for p63 staining, n=14 in naïve spheres; n=11 in inflamed spheres; error bar=SE; determinations were combined from 2–3 independent experiments.)

Table 1

Ratio of two types of spheres in naive and inflamed groups

	Naive	Inflamed
Solid spheres	79% (46/58)	58.6% (17/29)
Tubule-like spheres	21% (12/58)	41.4% (12/29)

Fisher's test, $p<0.0035$**